Supplemental Information

Vanadium Oxide Pillared by Interlayer Mg^{2+} Ions and Water as Ultralong Life Cathodes for Magnesium Ion Batteries

Yanan Xu, Xuanwei Deng, Qidong Li, Guobin Zhang, Fangyu Xiong, Shuangshuang Tan, Qiulong Wei, Jun Lu, Jiantao Li, Qinyou An, and Liqiang Mai

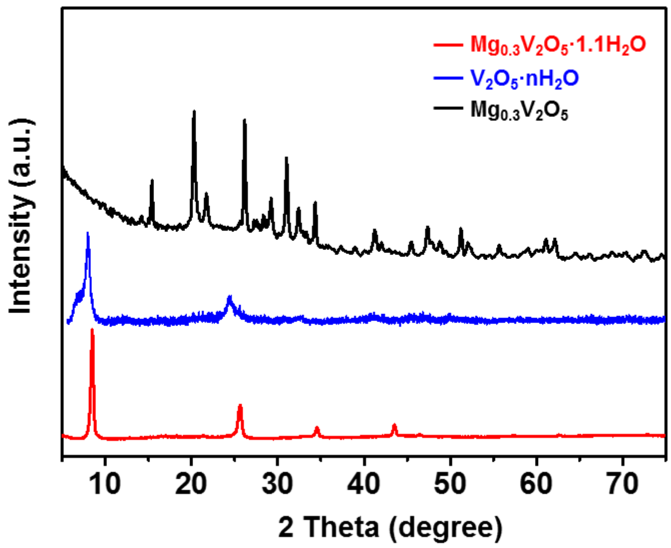

Figure S1. XRD diffraction patterns of $Mg_{0.3}V_2O_5 \cdot 1.1H_2O$, $V_2O_5 \cdot nH_2O$ and $Mg_{0.3}V_2O_5$.

Table S1. Inductively Coupled Plasma Optical Emission Spectroscopy (ICPOES) analysis of $Mg_{0.3}V_2O_5 \cdot 1.1H_2O$ and $Mg_{0.3}V_2O_5$.

Elements / Samples	Mg (W/%)	V (W/%)	Mg/V
$Mg_{0.3}V_2O_5 \cdot 1.1H_2O$	2.92	40.69	0.3/2
$Mg_{0.3}V_2O_5$	2.99	41.90	0.3/2

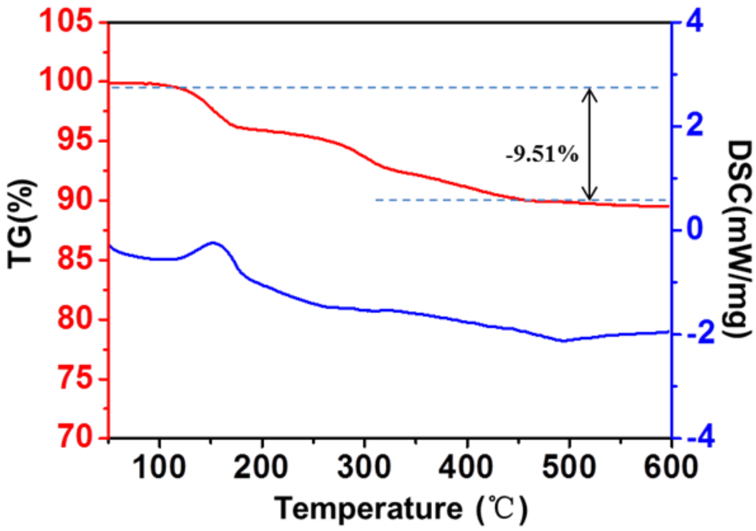

Figure S2. TGA-DTA analysis of the pristine $Mg_{0.3}V_2O_5 \cdot 1.1H_2O$. The $Mg_{0.3}V_2O_5 \cdot 1.1H_2O$ shows stepwise loss of lattice water corresponding to an overall 9.51% weight loss, equivalent to 1.1 molecule of water per formula unit.

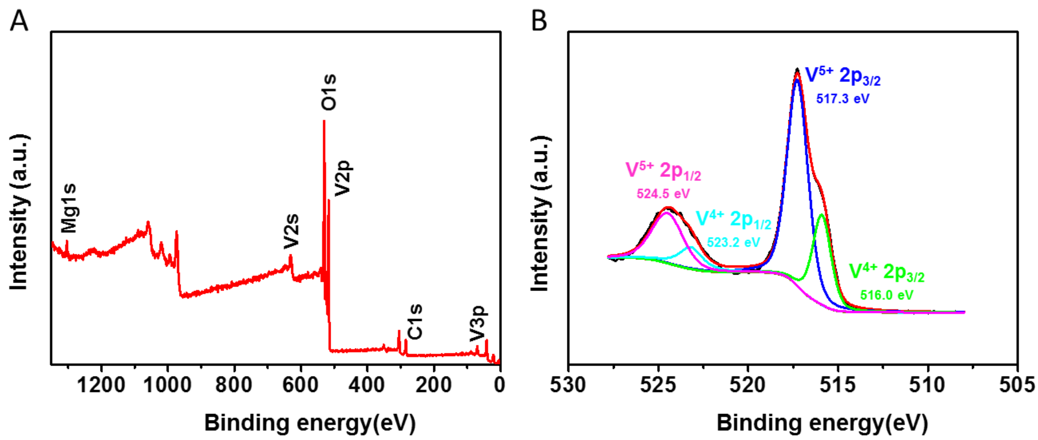

Figure S3. (A) Survey XPS spectrum and (B) high-resolution XPS spectrum of V2p peak for the resulting $Mg_{0.3}V_2O_5 \cdot 1.1H_2O$.

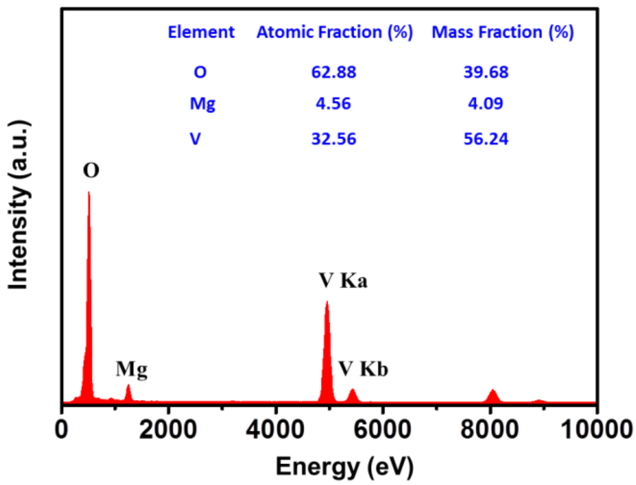

Figure S4. Energy dispersive X-ray (EDX) spectrum of the $Mg_{0.3}V_2O_5 \cdot 1.1H_2O$.

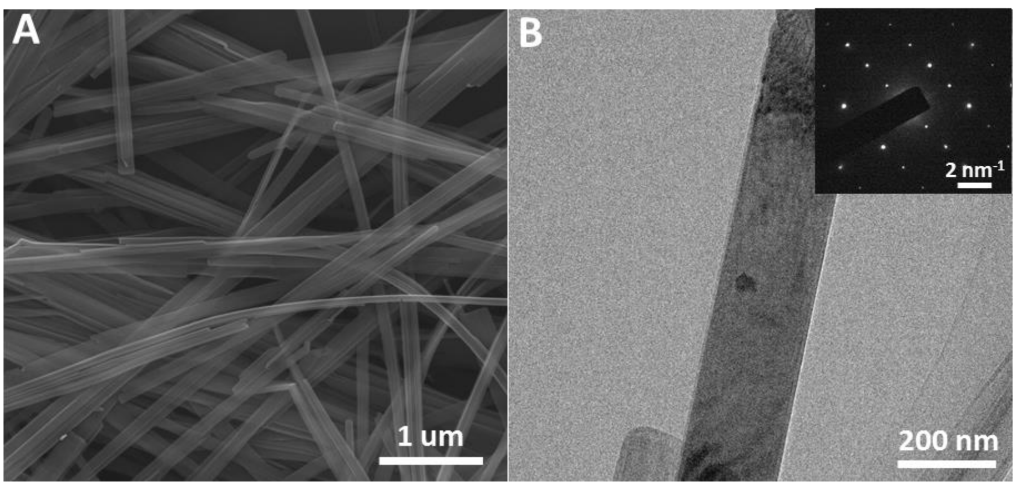

Figure S5. (A) FESEM image, (B) TEM images and (inset of B) SAED pattern of $V_2O_5 \cdot nH_2O$.

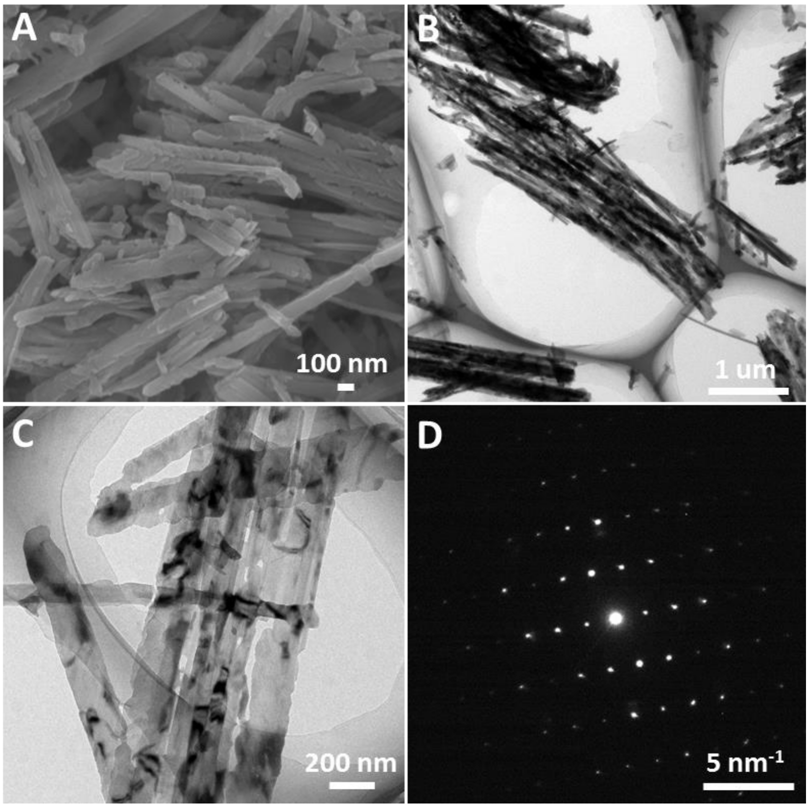

Figure S6. (A) FESEM image, (B,C) TEM images, (inset of C) HRTEM image and (D) SAED pattern of $Mg_{0.3}V_2O_5$.

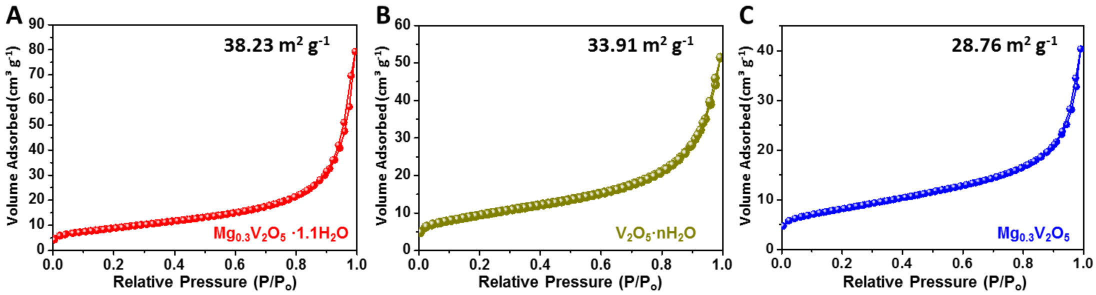

Figure S7. Nitrogen adsorption-desorption isotherms of (A) $Mg_{0.3}V_2O_5{\cdot}1.1H_2O$, (B) $V_2O_5{\cdot}nH_2O$ and (C) $Mg_{0.3}V_2O_5$.

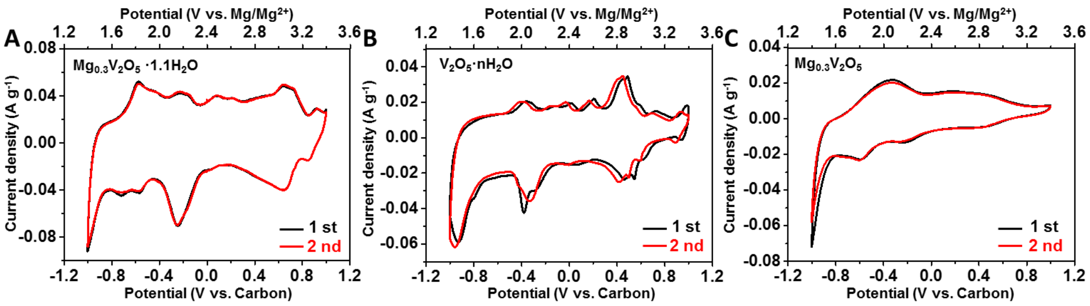

Figure S8. CV curves of (A) $Mg_{0.3}V_2O_5{\cdot}1.1H_2O$, (B) $V_2O_5{\cdot}nH_2O$ and (C) $Mg_{0.3}V_2O_5$ for the first two cycle at a scanning rate of 0.1 mV s^{-1} between 1.4 and 3.4 V vs. Mg/Mg^{2+}.

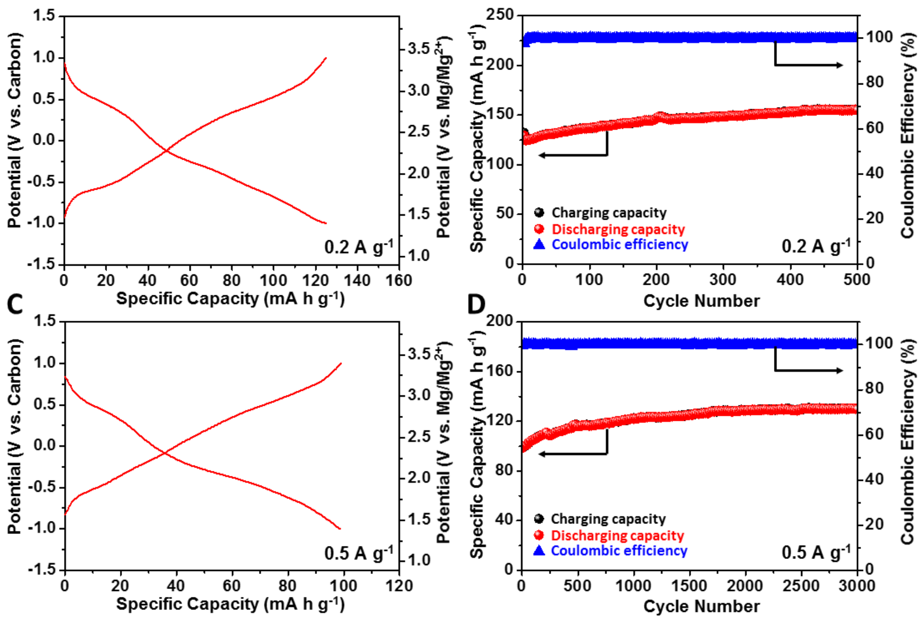

Figure S9. Discharge-charge curves (A,C) and cycling performances (B,D) of $Mg_{0.3}V_2O_5 \cdot 1.1H_2O$ at 0.2 and 0.5 A g^{-1}, respectively.

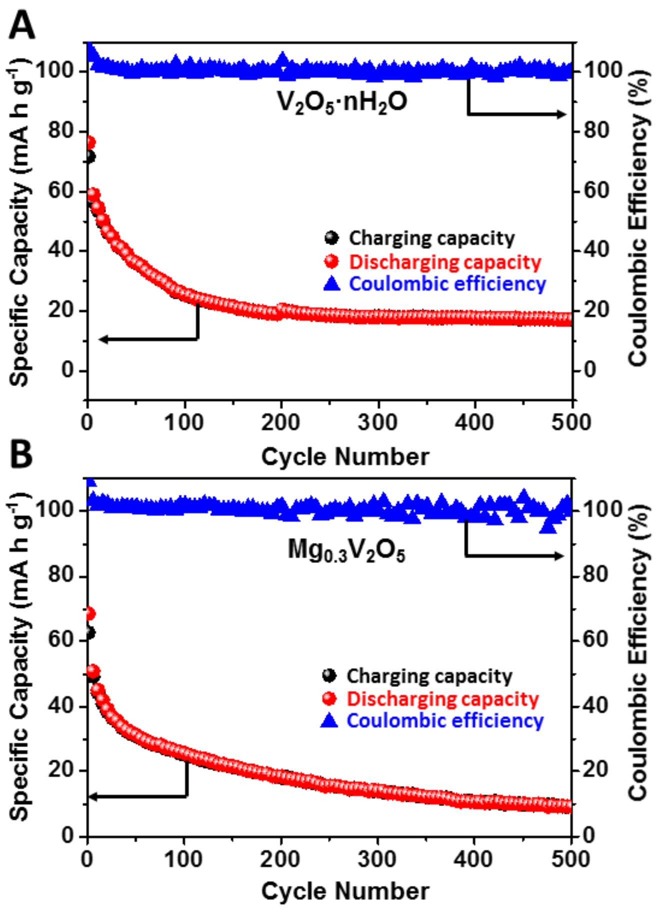

Figure S10. Cycling performances of (A) $V_2O_5 \cdot nH_2O$ and (B) $Mg_{0.3}V_2O_5$ at 0.5 A g^{-1}, respectively.

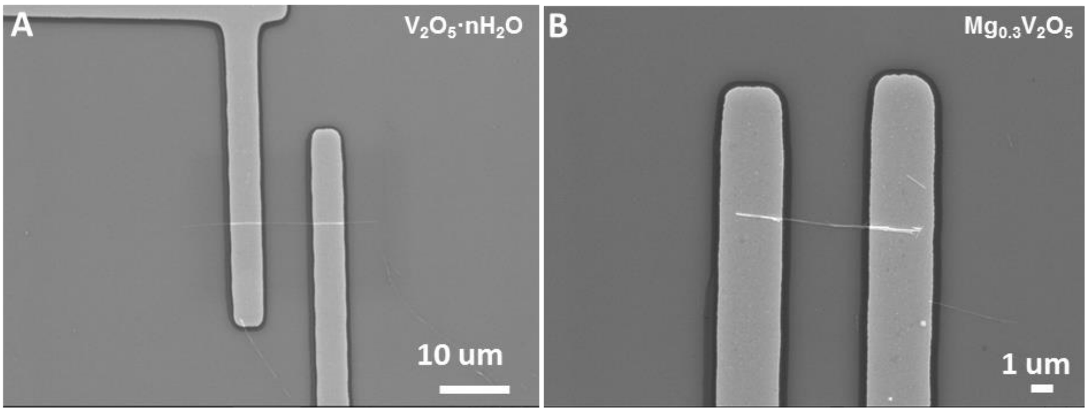

Figure S11. SEM images of the (A) $V_2O_5 \cdot nH_2O$ and (B) $Mg_{0.3}V_2O_5$ single nanowire devices, respectively.

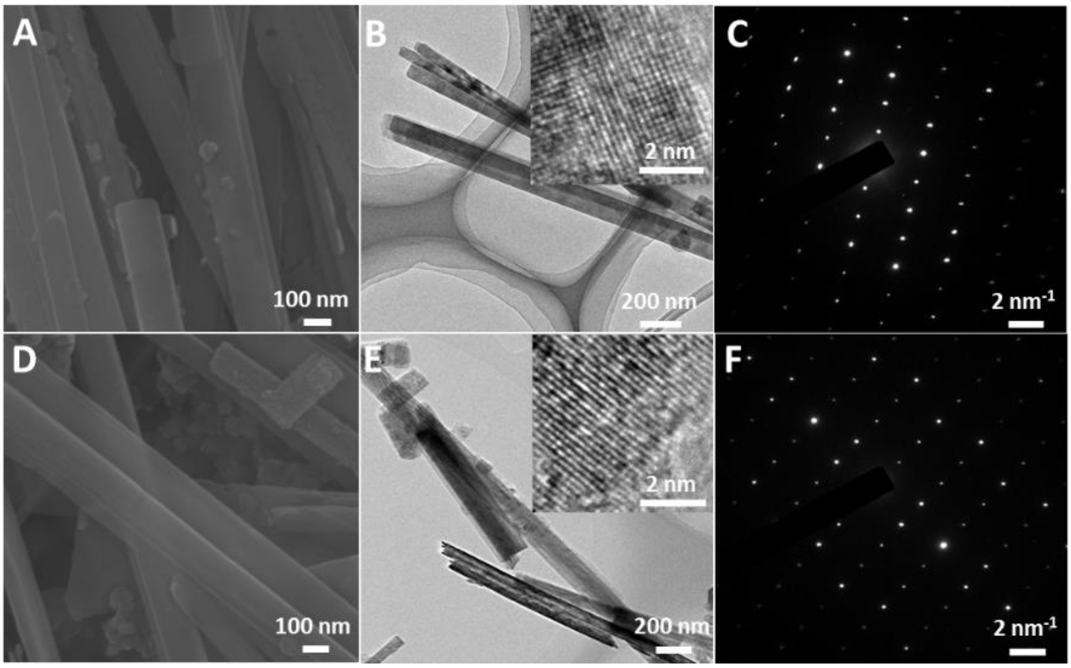

Figure S12. (A) SEM image, (B) TEM image, (insets of B) HRTEM image and (C) SAED pattern of $Mg_{0.3}V_2O_5 \cdot 1.1H_2O$ after 500 cycles at 0.1 A g^{-1}. (D) SEM image, (E) TEM image, (insets of E) HRTEM image and (F) SAED pattern of $Mg_{0.3}V_2O_5 \cdot 1.1H_2O$ after 10000 cycles at 1 A g^{-1}.

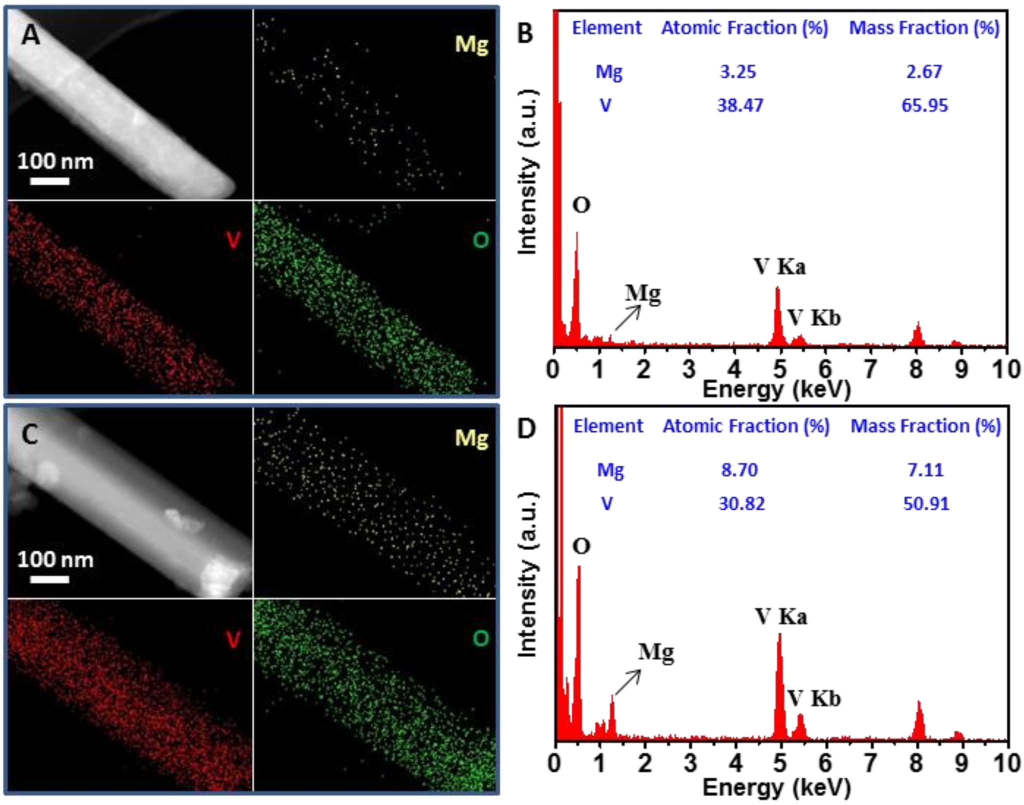

Figure S13. (A) TEM-EDX element mapping images of $Mg_{0.3}V_2O_5{\cdot}1.1H_2O$ nanowires at full charge state in 10th cycle, and (B) corresponding energy dispersive X-ray (EDX) spectrum. (C) TEM-EDX element mapping images of $Mg_{0.3}V_2O_5{\cdot}1.1H_2O$ nanowires at full discharge state in 10th cycle, and (D) corresponding energy dispersive X-ray (EDX) spectrum.

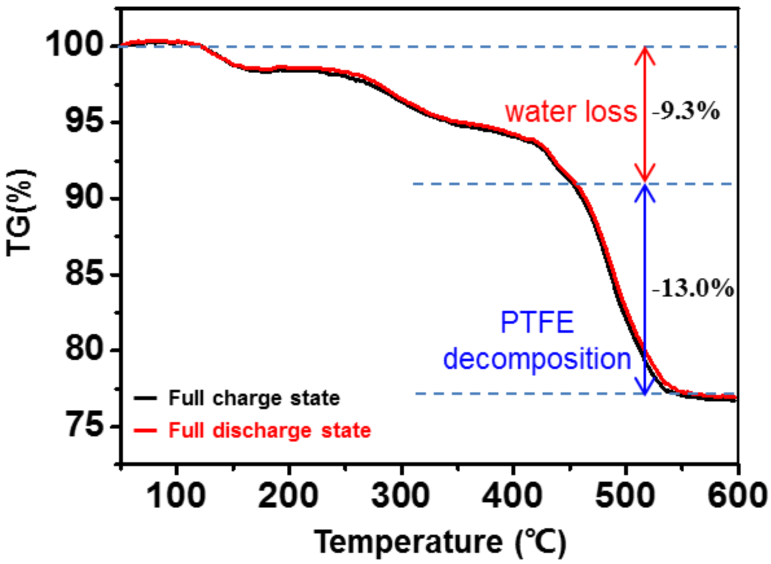

Figure S14. Thermogravimetry analysis (TGA) curves of $Mg_{0.3}V_2O_5{\cdot}1.1H_2O$ nanowires after charging and discharging.

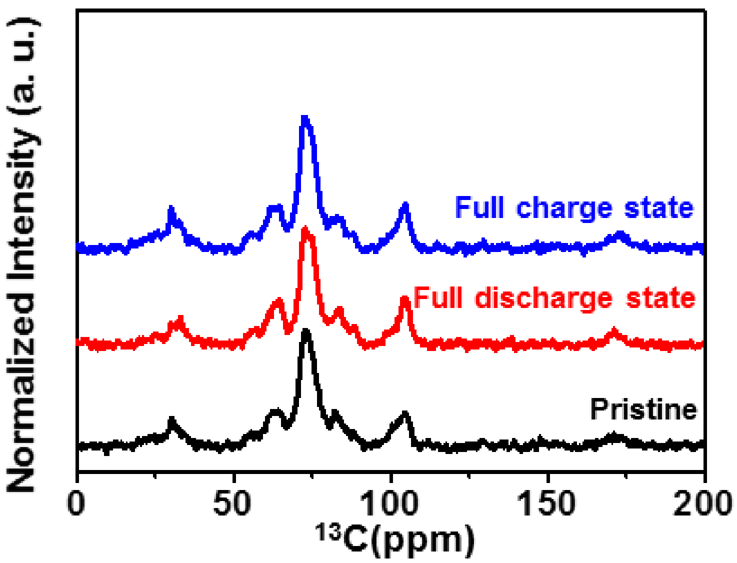

Figure S15. ^{13}C MAS NMR spectra collected for pristine $Mg_{0.3}V_2O_5 \cdot 1.1H_2O$ (black line), $Mg_{0.3}V_2O_5 \cdot 1.1H_2O$ after full discharging (red line) and full charging (blue line).

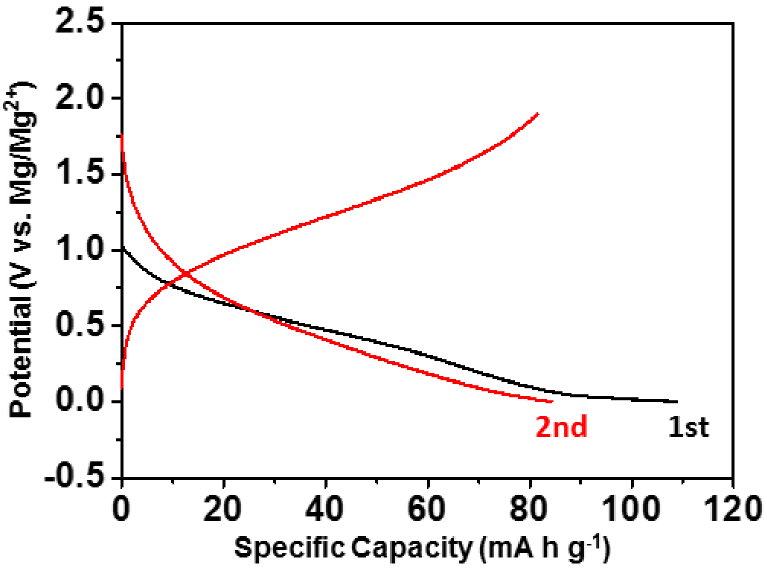

Figure S16. Discharge/Charge profiles of $Na_2Ti_3O_7$ in APC electrolyte at 20 mA g^{-1}. During the first discharge process, Mg^{2+} intercalation with irreversible Na^+ deintercalation ($Na_2Ti_3O_7 + Mg^{2+} + e^- \rightarrow MgNaTi_3O_7 + Na^+$). In subsequent charge/discharge processes, the reversible 0.5 M Mg^{2+} insertion−extraction occurs ($MgNaTi_3O_7 \leftrightarrow Mg_{0.5}NaTi_3O_7 + 0.5Mg^{2+} + e^-$). The calculated theoretical capacity is of 88 mA h g^{-1}, and the practical test is of 83 mA h g^{-1} in this work.

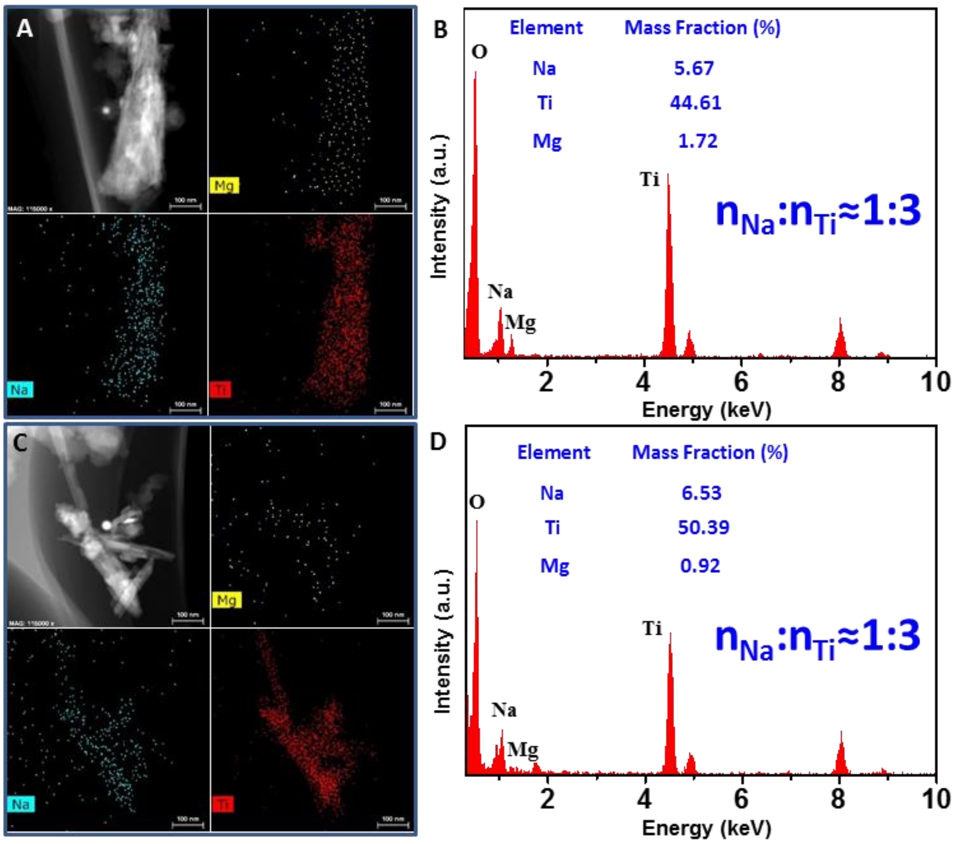

Figure S17. (A) TEM-EDX element mapping images of $MgNaTi_3O_7$ anode in charging state in $MgNaTi_3O_7/Mg_{0.3}V_2O_5 \cdot 1.1H_2O$ full cell, and (B) corresponding energy dispersive X-ray (EDX) spectrum. (C) TEM-EDX element mapping images of $MgNaTi_3O_7$ anode in discharging state in $MgNaTi_3O_7/Mg_{0.3}V_2O_5 \cdot 1.1H_2O$ full cell, and (D) corresponding energy dispersive X-ray (EDX) spectrum.

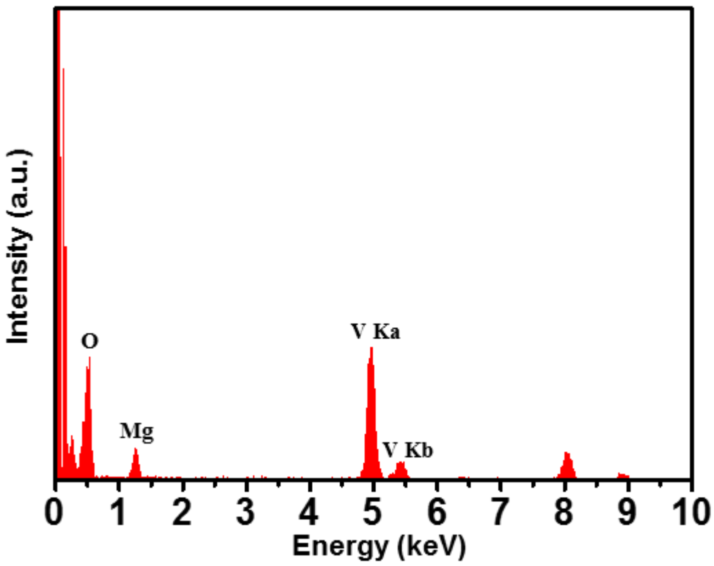

Figure S18. EDX spectrum of $Mg_{0.3}V_2O_5 \cdot 1.1H_2O$ cathode in discharging state in $MgNaTi_3O_7/Mg_{0.3}V_2O_5 \cdot 1.1H_2O$ full cell.